

A slit grating spectrograph for quantitative soft x-ray spectroscopy

T. Wilhein,^{a)} S. Rehbein, and D. Hambach

Forschungseinrichtung Röntgenphysik, Georg-August Universität Göttingen, Geiststr. 11, D-37073 Göttingen, Germany

M. Berglund, L. Rymell, and H. M. Hertz

Biomedical and X-Ray Physics, Royal Institute of Technology, S-10044 Stockholm, Sweden

(Received 30 September 1998; accepted for publication 12 October 1998)

In this article we describe a new slit grating spectrograph which is based on an e-beam written 10 000 linepairs/mm freestanding transmission diffraction grating. In combination with a thinned, back-illuminated charge coupled device (CCD), the spectrograph allows for real-time spectroscopy of laser-produced plasma x-ray sources within the wavelength region $\lambda=1\text{--}20$ nm. Calibration of grating and CCD allow for the possibility to measure absolute photon fluxes, currently within the wavelength region $\lambda=1\text{--}6$ nm. The compact spectrograph is easy to align and flexible in its use. Absolutely calibrated spectra were obtained from a liquid-jet laser-plasma source in the water window, with a spectral resolution $\lambda/\Delta\lambda\geq 330$ at $\lambda=3.37$ nm. A simple change in experimental geometry allowed single-shot spectra to be recorded with $\lambda/\Delta\lambda\geq 60$ at the same wavelength. In addition, spectra from this laser-plasma source were measured within the range $\lambda=9\text{--}20$ nm.
© 1999 American Institute of Physics. [S0034-6748(99)02203-0]

I. INTRODUCTION

Laser-produced plasmas promise to become bright soft x-ray sources for applications such as x-ray microscopy, photoelectron spectroscopy, and lithography.¹⁻⁶ To estimate exposure times for a particular experiment, the absolute spectral emission of the x-ray source must be determined. Additionally, in order to guarantee stable source operation, real-time control of the plasma parameters is needed. Soft x-ray spectroscopy is a powerful tool in the diagnostics of laser-produced plasmas and can provide the requested information. Various different spectrographs, such as grazing-incidence reflection-grating systems or pinhole grating spectrographs (with line densities up to 5000 linepairs/mm), have been developed to investigate the emission of laser-produced plasmas within the soft x-ray range.⁷⁻¹¹ However, to conduct real-time quantitative spectroscopy in a routine manner is still a challenging task. The compact slit spectrograph described in the present article relies on the developments in the field of diffractive x-ray optics. It is based on a freestanding transmission grating with 10 000 linepairs/mm mounted on a holder. This allows for an exchange of the slit or pinhole in order to choose between high collection efficiency at moderate spectral resolution for single-shot experiments (wide slit) and applications in which high spectral resolving power is needed (narrow slit). The grating is produced by electron beam lithography and successive nanofabrication processing. Quantitative real-time recording is provided by a calibrated thinned, back-illuminated charge coupled device (CCD) detector.

^{a)}Electronic mail: twilhei@gwdg.de

II. SPECTROGRAPH PROPERTIES AND SETUP

Pinhole and slit grating spectrographs are perhaps the simplest optical arrangements for spectroscopic experiments of which one can think. Figure 1 shows the basic scheme. The x-ray source projects a shadow of the grating-carrying pinhole onto the detector. This is then reproduced by grating diffraction for each wavelength at position $x=\lambda\cdot b/d$ in the detector plane, where b denotes the grating-detector distance, d the grating period, and λ the wavelength. The absence of a focusing element limits the spectral resolution $\Delta\lambda_g$ with respect to the size of the corresponding geometric shadow to (based on the notation in Fig. 1, compare, e.g., Ref. 7)

$$\Delta\lambda_g = d \left[\frac{D+q}{g} + \frac{D}{b} \right]. \quad (1)$$

However, the diffraction limited spectral resolution in the first diffraction order is given as $\Delta\lambda_d=\lambda/n$, where n =number of illuminated linepairs. One possibility to optimize the setup is to set $\Delta\lambda_g=\Delta\lambda_d$. In Eq. (1), D is the diameter when a circular pinhole is used or it is the extension perpendicular to the grating lines when a rectangular aperture (slit) is applied. The advantage of a slit of length L compared to a circular pinhole is that a higher collected solid angle Ω is achievable for a specific spectral resolution. The size of the 10 000 linepairs/mm gratings in use is $120\ \mu\text{m}\times 300\ \mu\text{m}$. In the near future, the length will be extended to $L\geq 1000\ \mu\text{m}$ for an enhanced collection efficiency. Typical values for the slit width vary from $D\approx 25\text{--}100\ \mu\text{m}$. In the present article a slit with $D=52\ \mu\text{m}$ was used. Thin metal filters (e.g., 200 nm Al) may be placed in front of the grating spectrograph to suppress scattered visible light. A thinned, back-illuminated CCD detects the spectrum nearly in real-

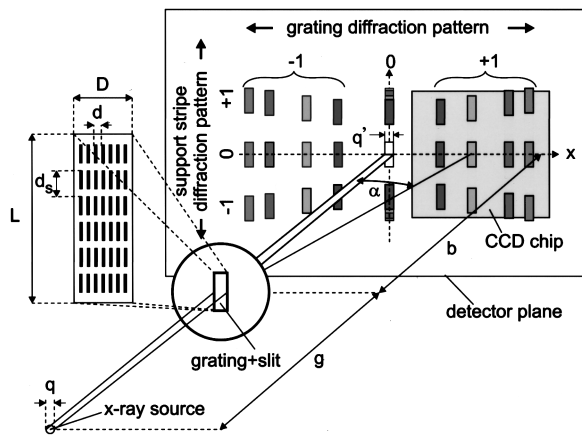


FIG. 1. Working principle of the SGS. The projection shadow of the slit is reproduced by grating diffraction for each wavelength. Aside from the regular diffraction pattern (the spectrum), mixed orders of grating and support stripe diffraction are observed.

time mode (read-out speed 40 kHz, 1024×1024 pixel of 24 μm size), and displays it on a computer screen with a delay of several seconds.

Due to the normal-incidence character of the slit grating spectrograph, this system is much easier to align than spectrographs which use grazing-incidence x-ray optics. In addition, the values for g and b can be chosen within a wide range. Thus, the system allows for optimization of setup geometry for a particular application without the necessity of running complex alignment procedures.

III. GRATING MANUFACTURING

The pattern of the freestanding grating is created by e-beam lithography (LION LV1 e-beam lithography system, Leica Microsystems Lithography GmbH, Jena).¹² Figure 2 shows a schematic of the process. To stabilize the structures and maintain the grating bars in place after nanostructuring, the grating pattern contains a support stripe structure perpendicular to the grating lines. The period of this support grating is $d_s = 1000$ nm with a duty cycle of 70% with respect to the transmissive fraction. The layer system prepared for the li-

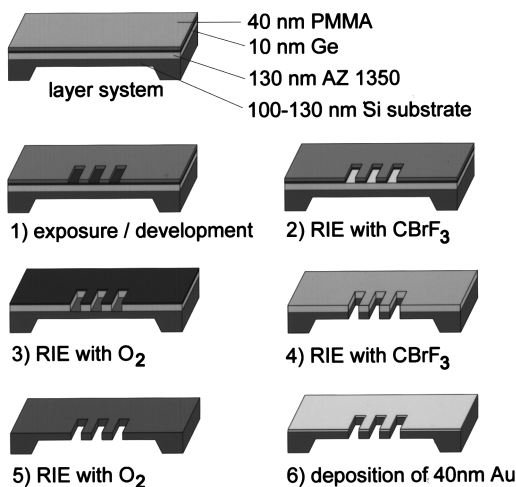


FIG. 2. Nanoprocessing of the freestanding diffraction grating.

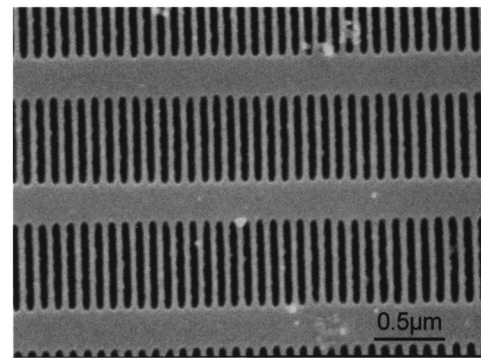


FIG. 3. Electron micrograph of a part of a freestanding diffraction grating with 100 nm d spacing and 1000 nm period support stripe structure.

thography progress consists of the substrate (100–130 nm thick Si), on which 130 nm photoresist (AZ 1350), 10 nm Ge and 40 nm electron resist poly(methylmethacrylate) (PMMA) are deposited. Following the e-beam exposure and development of the PMMA, the pattern is transferred into the Ge layer by reactive ion etching (RIE) with CBrF_3 and in the next step in the AZ 1350 with O_2 RIE. The resulting AZ 1350 structure serves as an etching mask for RIE of the Si substrate with CBrF_3 . After the removal of the etching mask with O_2 , ~40 nm Au is deposited by e-beam evaporation on the grating as the final step of the nanoprocessing. The Au layer supplies the absorption necessary to achieve reasonable diffraction efficiency within the lower wavelength region. In order to suppress even diffraction orders, the duty cycle is adjusted to $(50 \pm 5\%)$. Figure 3 displays an electron micrograph of a part of a 10000 linepairs/mm grating.

IV. MECHANICAL ASSEMBLY

To keep the spectrograph flexible and compact, a special grating/slit holder was developed, allowing for exchange of the slit without risking damaging of the grating. The complete holder consists of three parts: a main body made of Al, one holder for the grating, one for the slit (stainless steel). The main body contains two ball bearings mounted with their rotational axes parallel, yet separated by 1 mm (see Fig. 4). The grating and slit are glued to their holders so that they are located approximately 0.6–0.8 mm from the center. By mounting these holders in the ball bearings, the slit and grating are positioned with a distance of ~0.5 mm from each other. This configuration allows for the desired two-dimensional adjustment (slit-grating parallelism and lateral slit position perpendicular to grating lines) by rotating both the slit and grating holder in the ball bearings under microscope observation until one of the two matching positions is found and fixed (Fig. 4). With this compact arrangement, an alignment accuracy of less than 5 μm is easily achieved. The slit holder is equipped with a ring magnet which can hold a steel plate with a thin metal filter to block stray light from the laser. The assembly is completed by fixing the main body with the grating and slit onto a standard KF40 flange center ring. In the spectroscopy experiment, the holder is simply put between two 40 mm Ø tubes instead of an ordinary o ring at the desired distance to the source.

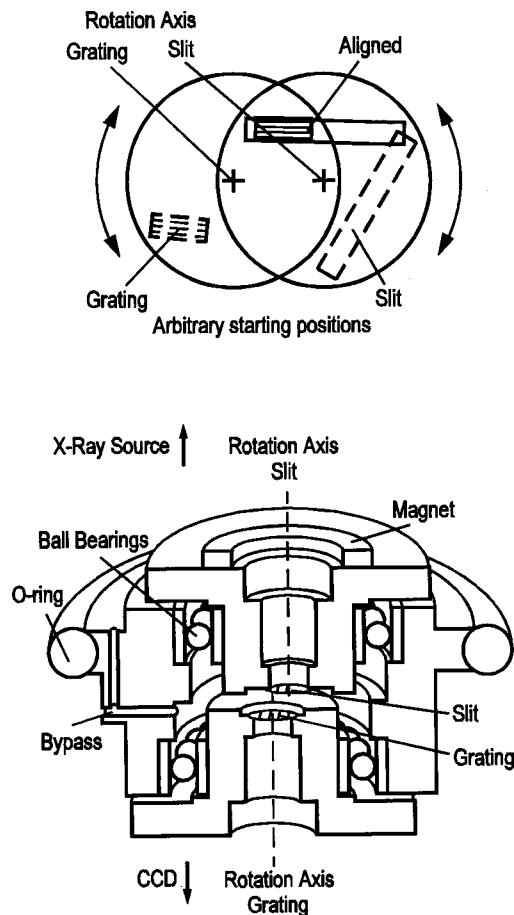


FIG. 4. Mechanical assembly.

V. CALIBRATION

The main goals of this work was to develop a compact spectrograph which would provide absolutely calibrated spectral measurements. Thus, the diffraction efficiency of the grating and the quantum efficiency of the CCD detector (Photometrics AT200L, equipped with Tektronix TK1024AB, thinned, back-illuminated CCD chip) had to be determined. The calibration procedures for the grating as well as for metal filters were carried out using the x-ray test chamber of the FE Röntgenphysik at the Berlin electron storage ring BESSY. Due to the existing monochromator setup of the x-ray test chamber, the spectral range for the calibration is currently limited to $\lambda=1-6$ nm. Figure 5 displays the measured values (symbols). The combination of Si and Au as absorbers leads to a nearly constant diffraction efficiency within the range 2–6 nm. A theoretical curve for the grating diffraction efficiency (solid line) was obtained by employing an algorithm based on Ref. 13. Assuming a thickness of 110 nm for the Si substrate and 40 nm for the Au layer, the calculated diffraction efficiency fits the measured data very well. Deviations between measured and calculated first order diffraction efficiencies can be explained by the fact that the duty cycle will not be exactly 50%. Measurement of the CCD quantum efficiency was performed at the radiometry beamline of the Physikalisch Technische Bundesanstalt at

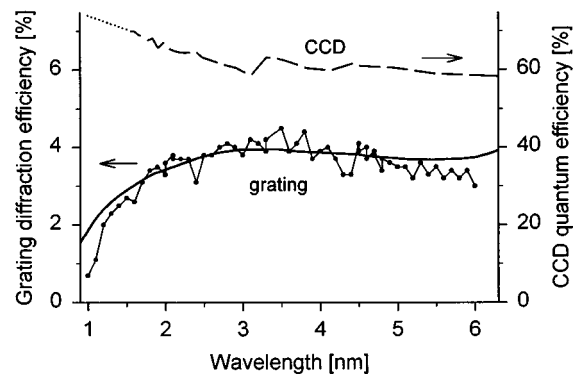


FIG. 5. Calibration curves obtained at BESSY. Symbols/left scale: measured data for the grating diffraction efficiency. Solid line/left scale: calculated values for 110 nm Si and 40 nm Au. Dashed line/right scale: measured CCD quantum efficiency. Dotted: extrapolation to shorter wavelength.

BESSY within the range $\lambda=1.5-20$ nm.¹⁴ Figure 5 shows the measured data (dashed) and extrapolations to 1 nm wavelength (dotted).

From the calibration procedures, the total uncertainty for measurements of photon numbers with the slit grating spectrograph (SGS) is estimated to be less than 30%.

VI. EXPERIMENTAL RESULTS

For the first experiments within the short wavelength region, $\lambda=1-6$ nm, a liquid jet-laser plasma source was used, running with ethanol as target liquid. The laser-plasma x-ray source is described in detail in Ref. 15. The driving laser was a frequency doubled Nd:YAG laser with 100 ps, 70 mJ, 10 Hz output (Continuum PYC61-C) focused to a 12 μm diam spot full width at half maximum (FWHM), resulting in an intensity of $\approx 5 \times 10^{14}$ W/cm² applied to the jet. In order to demonstrate the high spectral resolving power which is achievable with the SGS, a “long distance” geometry was chosen: $g=b=1550$ mm, $D=52$ μm , $d=100$ nm. Figure 6 shows a schematic of the setup. The absolutely calibrated ethanol spectrum recorded with this setup, given in numbers of photons per pulse, unit solid angle and 1 pm absolute wavelength interval, is displayed in Fig. 7. Emission lines of highly ionized oxygen and carbon are easily identified. Integration over 1000 shots results in a very good signal-to-

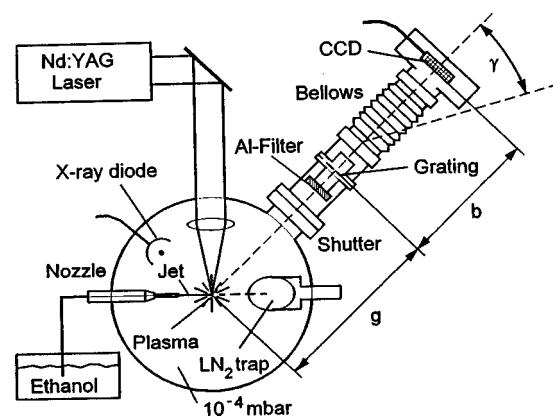


FIG. 6. Experimental arrangement used for the spectral measurements with the SGS.

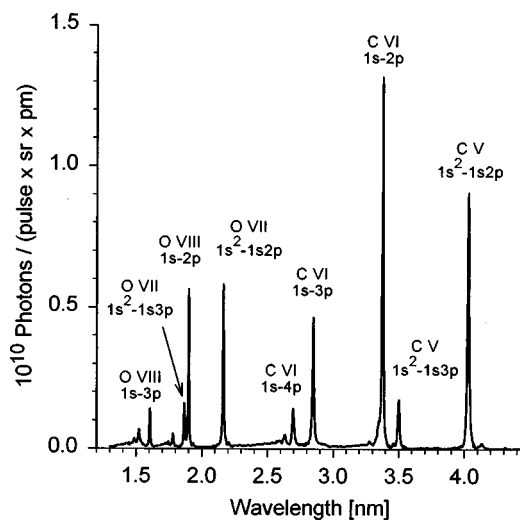


FIG. 7. Absolutely calibrated spectrum of the ethanol jet laser plasma source in the $\lambda=1.2\text{--}4.4$ nm range.

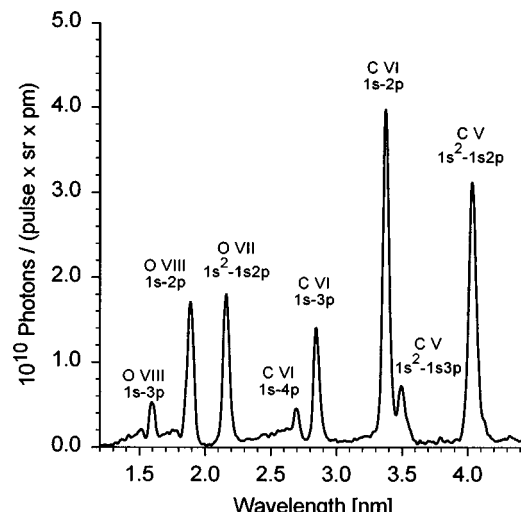


FIG. 8. Absolutely calibrated single shot spectrum (with prepulse).

noise-ratio (SNR). The measured width (FWHM) of the C VI $1s\text{--}2p$ line at $\lambda=3.37$ nm is used to determine the achieved spectral resolving power. From the experimental data, $\Delta\lambda=0.0100$ nm and hence $\lambda/\Delta\lambda=337$ was found. If both the geometrical and diffraction limit are taken into account, a theoretical value $\Delta\lambda_{\text{th}}$ can be calculated for comparison: Following Eq. (1) for $\lambda=3.37$ nm and the setup geometry (assuming an x-ray source size of $12\ \mu\text{m}$, Ref. 16) results in $\Delta\lambda_g=0.00748$ nm, whereas the diffraction limit gives $\Delta\lambda_d=0.00649$ nm. Applying the least square method yields $\Delta\lambda_{\text{th}}=\text{Sqrt}(\Delta\lambda_g^2+\Delta\lambda_d^2)=0.0099$ nm and $\lambda/\Delta\lambda_{\text{th}}=341$. This value fits the measured resolving power almost perfectly. The width of the line itself is expected to be dominated by Doppler broadening, which can be calculated to be $\lambda/\Delta\lambda\approx 2000$ and can therefore be neglected for this estimation. The smallest absolute linewidth value was found to be $\Delta\lambda=0.0082$ nm in the O VIII $1s\text{--}2p$ line at $\lambda=1.90$ nm.

The calibration of the spectrograph allows for the evaluation of absolute photon numbers and efficiencies of laser into x-ray energy conversion emitted in the different spectral lines. For the strongest lines in the spectrum of Fig. 7 the values are 1.7×10^{11} photons/(pulse \times sr) (0.15% conversion efficiency), 2.4×10^{11} photons/(pulse \times sr) (0.26%), 1.0×10^{11} photons/(pulse \times sr) (0.18%), 7.2×10^{10} photons/(pulse \times sr) (0.13%) for the C V $1s^2\text{--}1s2p$ ($\lambda=4.03$ nm), C VI $1s\text{--}2p$ (3.37 nm), O VII $1s^2\text{--}1s2p$ (2.16 nm), O VIII $1s\text{--}2p$ (1.90 nm) lines, respectively. The values for the conversion efficiencies are well in agreement with measurements on other laser plasma sources.¹⁷

By changing the distances g and b to $g=b=330$ mm, the photon flux density in the detector plane increases by a factor of $(3100/660)^2=22$, so that single-shot spectra can be recorded at a reduced SNR. For this measurement, a small intrinsic laser prepulse was added, resulting in an increased x-ray emission.¹⁷ Figure 8 shows a typical single-shot spectrum. The spectrum is now sampled with $\Delta\lambda=0.050$ nm, ($\lambda/\Delta\lambda=67$ at 3.37 nm), which is still sufficient to discriminate the principal lines in the spectrum, such as C VI $1s\text{--}2p$ and C V $1s^2\text{--}1s3p$ at 3.37 and 3.50 nm, respectively. The emis-

sion in the C VI $1s\text{--}2p$ line is now 1.2×10^{12} photons/(pulse \times sr) (1.27%), hence, the prepulse enhances the conversion efficiency by a factor of ~ 5 , which confirms previous measurements.¹⁶

For extensive single-shot investigations, one can take advantage of the slow scan readout properties of the two-dimensional CCD in the following way: Exposing the CCD during readout instead of the regular exposure time produces spectra shifted with respect to each other by a certain amount of rows on a single image due to the charge transfer in the CCD structure. With this method, we were able to record complete spectra ($\lambda=1\text{--}5$ nm) from up to 20 consecutive shots at 10 Hz, allowing to observe shot-to-shot fluctuations in the x-ray plasma emission with the SGS.

In a third experiment, the emission of the laser plasma source in the $\lambda=10\text{--}20$ nm region was investigated. Measurements within this spectral range benefit most from the freestanding character of the diffraction grating, since any support foil would introduce strong absorption. The geometry was in this case set to $g=690$ mm, $b=675$ mm, $D=52\ \mu\text{m}$, $d=100$ nm. The spectral range fitting to the CCD size (~ 24 mm) is then ~ 3.5 nm. For the recording of spectra within this wavelength range, the CCD camera, which is connected to the spectrograph with a bellows, was successively shifted in the dispersion direction in order to catch adjacent parts of the spectrum (Fig. 6). Figure 9 displays an ethanol spectrum recorded with this arrangement for $\lambda=9\text{--}21$ nm. The relative linewidth of the C VI $2s\text{--}3p$ line was determined to $\lambda/\Delta\lambda\sim 370$.

Identification of emission from Li- and Be-like ions is much more difficult due to their large number of lines with small wavelength separation.¹⁸ Especially when the spectrograph's zeroth order, marking the $\lambda=0$ position, cannot be recorded simultaneously with the spectrum, absolute wavelength determination is often a problem. Fortunately, the design of the support stripe grating allows for measuring wavelengths independently from zero order observation. Figure 10 shows a CCD image corresponding to the $\lambda=12.5\text{--}17.9$ nm region of an ethanol spectrum as displayed in Fig. 9.

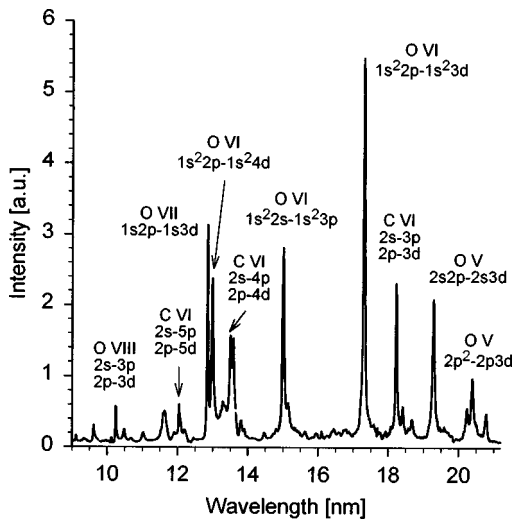


FIG. 9. Spectrum from the ethanol jet laser plasma source in the $\lambda=9\text{--}21$ nm range.

Above and below the spectrum created by the first order of the diffraction grating, mixed orders of diffraction grating (first order) and support stripe grating (\pm first order) can be seen. For better visibility, in order to enhance the weak mixed-order signal, the intensity scaling in Fig. 10 is extremely nonlinear. The angle between adjacent orders is given by $\tan(\chi) = (m_s \cdot d) / (m \cdot d_s)$ (m , m_s = diffraction orders for grating and support, respectively), which results in $\chi = 5.71^\circ$ for the described grating and $m_s = m = 1$. Knowing the grating-CCD distance, b , and measuring the distance Δx from the image file (cf. Fig. 10), the wavelength can be calculated with $\lambda = d_s \cdot \Delta x / b$. With this method, an accuracy of wavelength determination of less than 1% is easily achieved. This is in most cases sufficient to identify emission lines from laser produced plasmas. In the example of Fig. 10, the marked line is identified as arising from the O VI $1s^22p-1s^23d$ transition. In a similar way, the appearance of radiation produced by higher diffraction orders disturbing the spectrum can be detected. In this case a mixed order signal is

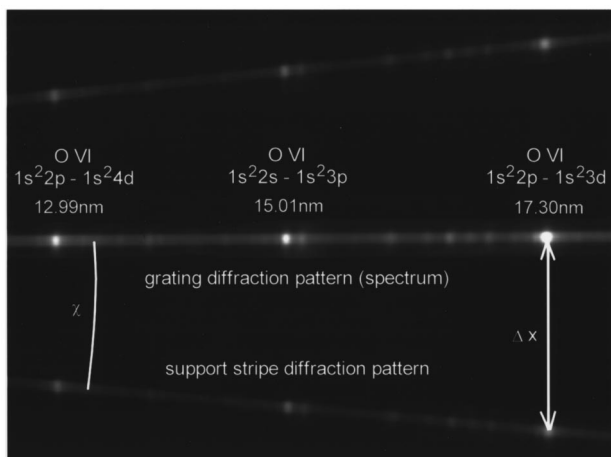


FIG. 10. CCD image taken with SGS in the $\lambda=12.5\text{--}17.9$ nm range in extreme nonlinear display scaling. The distance Δx between the spectrum and the mixed order $m=m_s=1$ can be used to determine absolute wavelength.

found at a different angle χ . For example, a signal arising from the third order of the diffraction grating results in $\tan(\chi) = d/3 \cdot d_s$, giving $\chi = 1.91^\circ$.

VII. DISCUSSION

The SGS operating with a freestanding 10 000 linepairs/mm transmission grating, created by e-beam lithography and nanofabrication processing, has proven to be a versatile instrument for spectral investigations of laser generated plasma x-ray sources. It is easy to set up and align, and allows for measurements of absolute photon numbers and conversion efficiencies. The achieved spectral resolution of $\lambda/\Delta\lambda \geq 330$ in the water window in the time integrating mode and $\lambda/\Delta\lambda > 60$ in single-shot experiments allow for real-time control and optimization of the x-ray emission from laser plasma sources. Further applications of the new SGS may include measurements and control of total exposure doses for, e.g., extreme ultraviolet and x-ray lithography as well as spectrally resolved measurements of, e.g., x-ray filter transmittances and detector efficiencies.

ACKNOWLEDGMENTS

The authors gratefully acknowledge G. Schmahl (FE Röntgenphysik, University of Göttingen) and Jamie Ettelson for their contributions. This work has been supported by the German Federal Ministry of Education and Research (BMBF) under Contract No. 13N6491, the EC Human Capital and Mobility program, and the Swedish Research Council for Engineering Sciences.

- ¹X-ray Microscopy and Spectromicroscopy, edited by J. Thieme, G. Schmahl, D. Rudolph, and E. Umbach (Springer, Heidelberg, 1998).
- ²L. Rymell, M. Berglund, and H. M. Hertz, Appl. Phys. Lett. **66**, 2625 (1995).
- ³See, e.g., OSA Trends in Optics and Photonics, Extreme Ultraviolet Lithography, edited by G. D. Kubiak and D. R. Kania (Optical Society of America, Washington, DC, 1996), Vol. 4.
- ⁴M. Berglund, L. Rymell, H. M. Hertz, and T. Wilhein, Rev. Sci. Instrum. **69**, 2361 (1998).
- ⁵M. Richardson, D. Torres, C. DePriest, F. Jin, and G. Shimkaveg, Opt. Commun. **145**, 109 (1998).
- ⁶H. Kondo, T. Tomie, and H. Shimizu, Appl. Phys. Lett. **72**, 2668 (1998).
- ⁷K. Eidmann, M. Kühne, P. Müller, and G. D. Tsakiris, J. X-Ray Sci. Technol. **2**, 259 (1990).
- ⁸W. Schwanda, K. Eidmann, and M. C. Richardson, J. X-Ray Sci. Technol. **4**, 8 (1993).
- ⁹J. F. Pelletier, M. Chaker, and J. C. Kieffer, J. X-Ray Sci. Technol. **6**, 359 (1996).
- ¹⁰T. Wilhein, D. Hambach, B. Niemann, M. Berglund, L. Rymell, and H. M. Hertz, Appl. Phys. Lett. **71**, 190 (1997).
- ¹¹J. Jasny, U. Teubner, W. Theobald, C. Wülker, J. Bergmann, and F. P. Schäfer, Rev. Sci. Instrum. **65**, 1631 (1994).
- ¹²B. Niemann, T. Wilhein, T. Schliebe, R. Plontke, O. Fortagne, I. Stolberg, and M. Zierbock, Microelectron. Eng. **30**, 49 (1996); T. Schliebe, Microelectron. Eng. **41/42**, 465 (1998).
- ¹³H. W. Schnopper, L. P. Van Speybroeck, J. P. Delvaile, A. Epstein, E. Källne, R. Z. Bachrach, J. Dijkstra, and L. Lantward, Appl. Opt. **16**, 1088 (1977); E. M. Gullikson, The diffraction efficiency of a transmission grating, http://www-cxro.lbl.gov/optical_constants/.
- ¹⁴T. Wilhein, D. Rothweiler, A. Tusche, F. Scholze, and W. Meyer-Illse, in X-ray Microscopy VI, edited by V. V. Aristov and A. I. Erko (Bogorodskii Pechatnik, Chernogolovka, Russia, 1994), p. 470.
- ¹⁵L. Rymell and H. M. Hertz, Opt. Commun. **103**, 105 (1993); H. M. Hertz,

- L. Rymell, M. Berglund, and L. Malmquist, Proc. SPIE **2523**, 88 (1995); L. Malmquist, L. Rymell, M. Berglund, and H. M. Hertz, Rev. Sci. Instrum. **67**, 4150 (1996).
- ¹⁶M. Berglund, L. Rymell, and H. M. Hertz, Appl. Phys. Lett. **69**, 1683 (1996).
- ¹⁷S. Bollanti, R. A. Cotton, P. Di Lazzaro, F. Flora, T. Letardi, N. Lisi, D. Batani, A. Conti, A. Mauri, L. Palladino, A. Reale, A. Ya. Faenov, T. Pikuz, and A. Oesterheld, Proc. SPIE **2523**, 70 (1995).
- ¹⁸see, e.g., R. L. Kelly, Atomic and Ionic UV/VUV Linelist, <http://cfa-www.harvard.edu/amp/data/stats/kelly.html>.